Available online at www.sciencedirect.com

ScienceDirect

Ceramics International 40 (2014) 2933–2942

CERAMICS INTERNATIONAL

www.elsevier.com/locate/ceramint

Investigation of mechanical behavior of CPC/bone specimens by finite element analysis

Tao Yu[a,b,1], Xuan Liu[a,1], Jiandong Ye[b,*], Ming Zhang[a,**]

[a]*Interdisciplinary Division of Biomedical Engineering, The Hong Kong Polytechnic University, Hung Hom, Kowloon, Hong Kong SAR, China*
[b]*Key Laboratory of Specially Functional Materials of Ministry of Education and School of Materials Science and Engineering, South China University of Technology, Guangzhou 510641, China*

Received 9 September 2013; received in revised form 4 October 2013; accepted 4 October 2013
Available online 11 October 2013

Abstract

Calcium phosphate cement (CPC), as an important injectable biomaterial, is extensively used for bone repair in clinical application. If mechanical properties of CPC match well with that of bone tissue, it can create an appropriate mechanical environment for bone repair. In our study, the objective was to investigate the responses of bone tissue to CPC in different series of elastic modulus combinations. Finite element analysis (FEA) was applied to calculate the stress/strain on CPC-bone specimens and to further forecast the potential risky area. The predicted results indicated that CPC materials and bone tissue had different stress distribution patterns under the same loading condition. For CPC material, the Von Mises Stress peak occurred in the bone–cement joint area; while for bone tissue, the risky area was located at the bridge area among trabecular bones. The porous and loose structure of cancellous bone induced a greater Von Mises Stress in bone tissue. Quantitative analysis indicated that stress/strain distribution was directly correlated with the elastic modulus of material. When Young's modulus of bone and CPC was 1 GPa and 6.10 GPa respectively, the optimal stress matching between bone and CPC was achieved. In sum, this work confirmed that FE modeling was the ideal method for predicting fracture behavior of bone–CPC specimen both qualitatively and quantitatively.

Keywords: Biomaterial; Bone repair; Finite element analysis

1. Introduction

Recently, minimal invasive surgery has received increasing attention in craniofacial, dental, and orthopedic application, because it is less aggressive than the classic surgical method. Self-setting biomaterials have a great potential in minimal invasive surgery [1]. The demand of biomaterials for minimal invasive surgery has induced the development of self-setting bone cement as injectable and/or moldable bone substitute [2–4]. CPC, as a highly promising bone substitute material, has attracted growing attention from scientists and surgeons recently, because of its injectability, self-setting property, easy plasticity, and good biocompatibility [5–8]. Given CPC's primary mechanical property, it can be used to support bone tissue, and its mechanical support can decrease the pain of patients. However, mechanical properties of CPC are not as good as that of polymethylmethacrylate (PMMA). PMMA has been used for approximately one hundred years clinically. Given that PMMA is non-degradable, CPC has better prospects in clinical application. Therefore, researchers have focused on improving mechanical properties of CPC for years [10–15]. CPC is usually injected into human trabecular bone, which means that CPC's strength should match the mechanical requirements of the local trabecular bone [9]. Success of bone repair is up to the following two points: whether materials can appropriately integrate with its surrounding tissues; and whether the implanted materials can fulfill biomechanical functions of native tissues. As it is known, bones will adapt their shape, density and/or internal architecture (in case of trabecular bone) to changes in loading condition [16,17].

*Corresponding author.
**Corresponding author. Tel.: +852 2766 4939.
E-mail addresses: jdye@scut.edu.cn (J. Ye), ming.zhang@polyu.edu.hk (M. Zhang).
[1]T. Yu, X. Liu equally contributed to this work

0272-8842/$ - see front matter © 2013 Elsevier Ltd and Techna Group S.r.l. All rights reserved.
http://dx.doi.org/10.1016/j.ceramint.2013.10.018

Table 1
Synthesis condition combination of as-processed ACPs.

ACP	*Ca/P* ratio	Milling time (h)	Additive
ACP-1	1.33	2	–
ACP-2	1.67	6	–
ACP-3	1.33	4	–
ACP-4	1.67	4	Strontium carbonate 15 wt%

In case that implanted material exceeds the stress that bone can bear, risk of secondary bone fracture will increase. Nowadays, skeletal biomechanics have been focused on how skeletal tissues are produced, maintained and adapted to biophysical stimuli in environment as an active response, which is currently known as mechanobiology [18]. During the bone repair process, effects of mechanical factor are important. Thus, how CPC's strength will match the mechanical requirements of trabecular bone needs to be verified through further study.

It is difficult to use traditional material tests to characterize the mechanical responses of CPC to bone tissue in vivo. Nowadays, with the development of computer technology, FEA applied to organic structures is one of the most promising area of biomechanical and biomaterial researches. Particularly, FEA has been proven effective in predicting the behavior of complex structures, such as bone–cement interface [19], dentin-postinterface [20] and tissue engineering scaffold [21]. The basic concept of FEA is the subdivision of mathematical model into a finite number of discrete elements. Through the solution of FEA, a great deal of insight into the internal stress distribution and deformation of the structure can be provided and complex material properties in modeling structures can be handled. The use of micro-imaging reconstruction and micro-finite element method to design CPC scaffold has been suggested previously [22], but it has not been applied to injectable CPC and the micromechanical behavior of bone–CPC interface.

Therefore, the objective of our work is to use finite element analysis (FEA) to calculate the stress/strain distribution in CPC/bone specimen, and thereby estimate their mechanical behavior under different loading conditions. The primary goals are: (1) to assess the local deformation and damage development in bone–CPC specimens under selected levels of uniaxial compression; (2) to evaluate the mechanical response to loading compression on the interface of CPC and bone. With the insightful information, CPC preparation can be optimized to provide an appropriate support in vivo, and it is an essential task to characterize and predict the mechanical behavior of the complex three-dimensional (3D) structure.

2. Materials and experiments

2.1. Materials preparation

In this work, CPC was prepared by mixing amorphous calcium phosphate (ACP) and dicalcium phosphate [23]. Four kinds of CPC were prepared: CPC-1, CPC-2 and CPC-3 were prepared by mixing ACP (1, 2, 3) and dicalcium phosphate with the weight ratio of 1:1; CPC-4 was prepared by mixing ACP-4 and dicalcium phosphate with the weight ratio of 2:1 (detailed in Table 1). The deionized water and cement powders were mixed in a mortar to obtain a paste with workable consistency, using a liquid/powder ratio of 0.4 mL/g. The paste was molded at 24–26 °C and 40–50% humidity. The cement specimens were stored in an incubator at 37 °C and 97% humidity.

Bovine trabecular bones were harvested from fresh iliac crest and used to mix with CPC paste to create bone–cement composite samples. The rectangular bone coupons were machined to size and cleaned to remove fatty tissues. The CPC slurry was placed on the surface of bone coupon to form a bone–cement interface following a procedure of Tozzi et al. [19]. The bone–cement specimen was stored for setting in an incubator at 37 °C and 97% humidity. The processed samples were used for micro-CT scanning.

2.2. Setting time measurements

The setting times of cements were measured according to the international standard ISO9917 for dental water-based cement. Ninety seconds after the end of mixing the CPC powders with liquid, the indenter (300+5 g in mass, 1+0.05 mm in diameter of the needle) was carefully lowered vertically onto the surface of cement and allowed to remain there for 5 s. Initial setting occurred when a 1 mm needle penetrated 25 mm into cement paste. Final set occurred when there was no visible penetration. Each test was repeated five times and the average value was calculated.

2.3. Compressive strength tests

Steel cylindrical molds with an inner diameter of 6 mm and a height of 12 mm were used to prepare the cement columns for compressive tests. The compressive strength of the columns were measured using an Instron 5567 testing machine (INSTRON, Britain) at a crosshead speed of 0.5 mm min^{-1}. Each measurement was repeated 5 times and the average value was calculated. The Young's modulus of CPC was calculated by the linear elastic constitutive law (E=tensile stress/tensile strain) [24,25].

2.4. Micro-CT image acquisition

Micro-CT image was used to identify submicron structures for materials. The prepared specimen (scanning dimension: 10 mm × 2 mm × 10 mm) was scanned using viva CT 40 scanner (SCANCO Medical AG, Brüttisellen, Switzerland). The scanner was set at a spatial resolution of 40 μm and a slice thickness of 20 μm to acquire the micro-architectures of the bone–ceramic complex. The system was set to a voltage of 70 kV and a current of 110 μA. The scanning direction was perpendicular to the bone–ceramic interface.

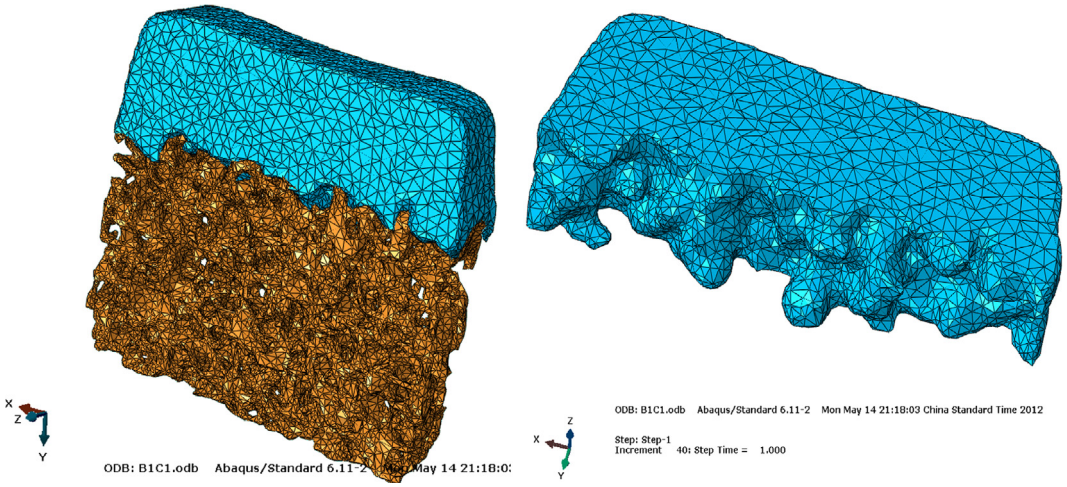

Fig. 1. The finite element model of bone–cement specimen.

Table 2
Setting times, compressive strength and Young's modulus of CPC groups.

CPC	Initial setting time (Min)	Final setting time (Min)	Compressive strength (MPa)	Young's modulus (GPa)
CPC-1	13 ± 0.9	21 ± 1.1	6.48 ± 0.5	0.54 ± 0.04
CPC-2	11 ± 1.0	20 ± 0.9	17.80 ± 0.5	1.48 ± 0.04
CPC-3	18 ± 1.0	44 ± 1.0	27.26 ± 0.3	2.27 ± 0.02
CPC-4	24 ± 3.4	42 ± 1.7	74.90 ± 2.3	6.10 ± 0.02

Table 3
Young's modulus combination between bone and cement.

	CPC-1 (0.54 GPa)	CPC-2 (1.48 GPa)	CPC-3 (2.27 GPa)	CPC-4 (6.10 GPa)
Bone 1 (1 GPa)	B1C1	B1C2	B1C3	B1C4
Bone 2 (5 GPa)	B2C1	B2C2	B2C3	B2C4

2.5. Finite element (FE) model establishment

The micro-CT images of the specimen were imported into MIMICS v14 software (Materialise, Leuven, Belgium) for geometry reconstruction and mesh. MIMICS wrap tool was used to distinguish small details of the trabecular bone. The segmentation of bone tissue and CPC was manually differentiated through the threshold gray levels in Mimics v14. ABAQUS package v6.11 (Dassault Systems Simulia Corp., Providence, RI, USA) was used for subsequent FE analysis. The model was meshed with tetrahedral elements. The element size was determined to be approximately 0.25 mm in both the bone and cement through convergence tests. The FE model of the bone–cement complex consists of 77,713 elements and 25,603 nodes. The finite element model of bone–cement specimen was shown in Fig. 1. Linear elastic constitutive law [45] was applied for bone tissue and cement, separately. Trabecular bones with different Young's modulus present different mechanical characteristics [24–29,36]. In our study, a chosen value of Young's modulus was given in bone tissue, and we figured out whether the change of Young's modulus for materials would affect the stress distribution between material and trabecular bone or not. The parallel experiments were also designed to figure out whether the change of values of Young's modulus for the trabecular bone will affect the stress distribution between material and trabecular bone or not (Table 3). The elastic properties were defined by giving Young's modulus, E, and Poisson's ratio, ν. In this study Young's modulus of 1, 5 GPa [28,29] was assigned to the bone respectively, with combinations of different material parameters of the cement (Table 3). These elastic properties were used as input for the FE simulations. Poisson's ratio of 0.3 [30] was assigned to both the bone and cement. The interaction between the bone and cement was modeled using tie constraint. In the stress test of material sample, the upper and lower surfaces of samples were polished to make them paralleled surface. And the pressure of vertical direction alone was tested in our study. Therefore, the base of sample was fixed and pressure on its horizontal surface was varied in our model, in order to get statistics which is in line with measurement.

Two loading conditions were applied to CPC/bone specimens (shown in Fig. 2). The Von Mises Stresses in bone, cement and the bone–cement interface were compared among different groups of Young's modulus combinations. For both of the bone and cement, any element with a Von Mises Stress higher than the material yield stress was regarded as damaged. During the simulation of the uniaxial compression tests, the Von Mises Stress was examined at every increment and analyzed to investigate the element deformation in compression scale.

3. Results

CPC was first presented by Brown and Chow in 1986 [31,32], which was composed of one or more calcium orthophosphates. After it was mixed with liquid phase, CPC could form a self-setting paste and harden within human body. CPC setting was the result of dissolution and precipitation process, and the precipitated crystals were responsible for

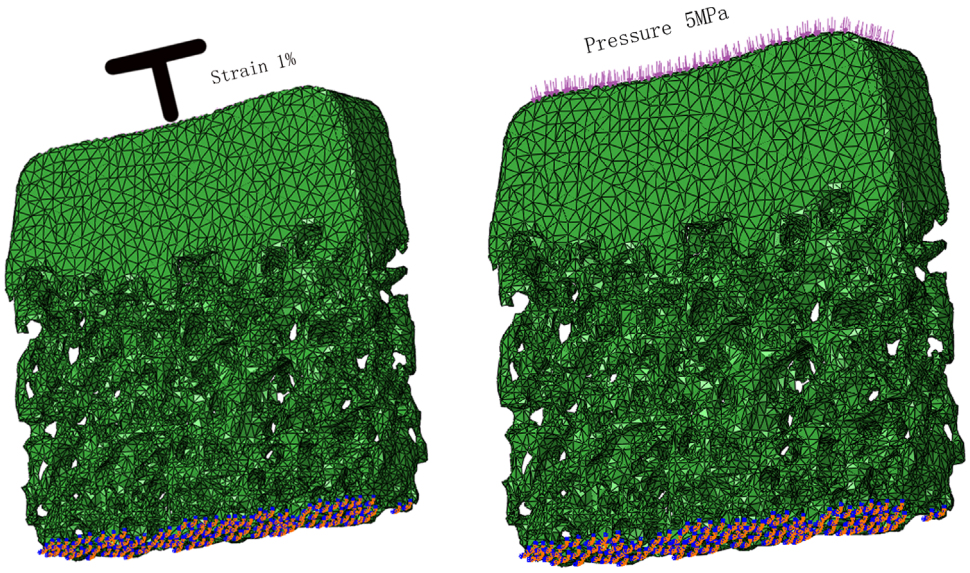

Fig. 2. Setting of the boundary conditions and loading: (A) the displacement of 1% compressive strain was applied to each trabecular cube on the vertical direction and (B) the constant pressure (5 MPa) was applied on the top surface of the sample. The bottom of the sample was fixed in both condition A and B.

cement hardening [33,34]. Generally speaking, CPC's duration of hardening should be no less than the time a surgeon needs to perform implantation, and no more than it, so there will be no delay in operation. Ideally, appropriate mechanical strength should be achieved within minutes after the initial setting. The method to assess the rate of a cement hardening was to measure its setting time and compressive strength, which was the most commonly used in tests. Table 2 summarizes different setting times and compressive strength of CPC. The initial setting times of all the CPC were less than 25 min; even the longest setting time of CPC-3 was less than 45 min. Table 2 demonstrates different compressive strengths and Young's modulus of CPC. Different material parameters of CPC were used as input for FE simulations (Table 3). CPC was set as a compact structure in FE model due to its dense structure. Fig. 1 exhibits the finite element model of bone–CPC specimens. Two loading conditions were applied to CPC/bone specimens (Fig. 2), which were strain mode and stress mode. And 1% strain was regarded that it was damaged [35].

Figs. 3–5 exhibit the stress distribution of specimens under damaged condition. In Fig. 3, CPCs are assigned with Young's modulus of 0.54, 1.48, 2.27 and 6.1 GPa. Applying 1% compressive strain, the Von Mises Stress distribution of specimens were trending up with the increment of CPC's Young's modulus. FE simulation predicted that bone was the major risky area. Fig. 3 exhibits that bone endures more stress than CPC; for CPC, more stress appears on the interface between CPC and bone; for bone, the bridge connecting bone trabecular units endures the more stress.

Fig. 4 indicates the local Von Mises Stress distribution of B2Cx series under loading condition of A. In B2Cx series, the elastic modulus of bone was set at 5 GPa. Under the same test scale, B2Cx series exhibit greater stress value than B1Cx series, and the Von Mises Stress distribution of specimens is also trending up with the increase of CPC's Young's modulus. The reason is that greater loading force is needed on the surface of CPC in order to reach the critical condition. FE prediction in Fig. 4 demonstrates the similar stress distribution with that in Fig. 3.

Fig. 5 exhibits a magnified view of stress distribution on the interface of bone and cement. Under the strain mode, interface demonstrates the greatest stress value in CPC. Stress value of CPC is trending up with the increase of CPC's elastic modulus. There is concentration of stress on the interface.

In clinical application, stress mode is the most commonly used loading condition. In stress mode, a persistent loading is applied on repair material. Fig. 6 exhibits the stress distribution of B1Cx series under the stress mode with 5 MPa. In B1Cx series, CPC's elastic modulus has a minor effect on its stress distribution. The bone tissue bears more stress, compared with CPC. The stress on bone predicted by FE modeling is trending up with the increase of CPC's elastic modulus.

Fig. 7 exhibits the stress distribution of B2Cx series. Compared with the results in Fig. 6, bone in Fig. 7 bears more stress. The results indicate that the stress on bone is trending up with the increase of bone's elastic modulus, but the stress distribution of CPC is trending down with it. The same results occurred in the test of bone–CPC interface.

Fig. 8 exhibits model of bone–CPC specimen with three transverse planes, which are chosen to calculate the average Von Mises Stress and strain quantitatively. Fig. 9 exhibits the quantitative stress distribution on different transverse planes. Under the persistent loading pressure of 5 MPa, the average stress value in B1Cx and B2Cx series is less than 3.5 MPa. The elastic modulus of material has a minor effect on the average stress of plane (a) and plane (c). In B1Cx series, the stress of plane (b) in CPC is trending up with the increase of CPC's elastic modulus, but the stress of plane (b) in bone is opposite. Results in B2Cx series are similar with B1Cx. The stress values of bone at the interface of B1Cx series are less

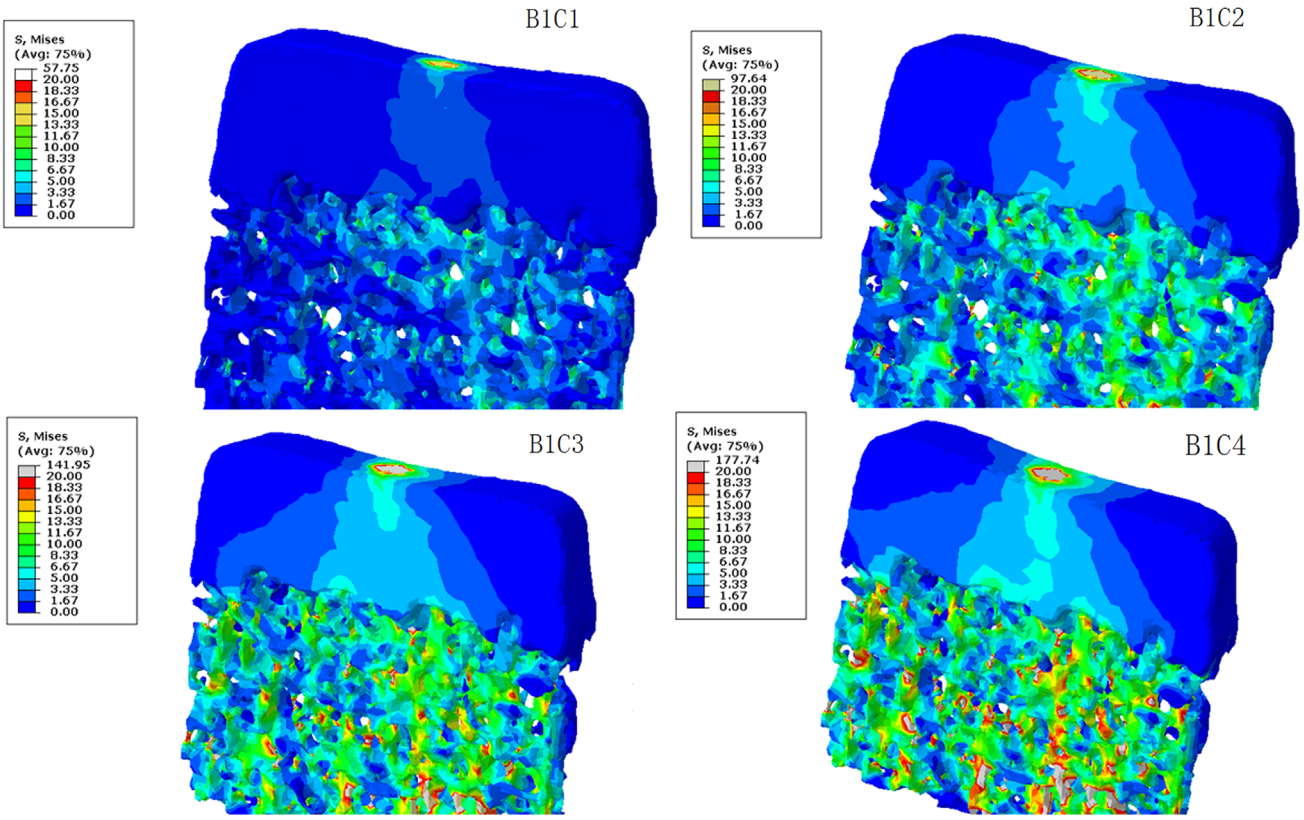

Fig. 3. The stress distributions on B1Cx series predicted from the FE model under the loading condition A. Cx: C1-C4.

than that in B2Cx series. Fig. 10 exhibits the quantitative average strain on different transverse planes. Under the surface pressure of 5 MPa, the strain value of CPC section is less than that of bone section. The elastic modulus has a great effect on the strain distribution of plane (a) and plane (b1) in CPC. For plane (b2) and plane (c), the strain value of bone in B1Cx series are larger than B2Cx series.

4. Discussion

The mechanical properties of bone is up to its composition and structure, but the composition of living tissues is not stable, and it changes with factors such as mechanical environment, age, disease, nutrition and so on [36]. The interdependency of mechanical properties and microstructure is so important that it is one of the fundamental objectives of materials science to understand mechanical properties of the tissue-implanted material complex in clinical application. In 1959, Vose and Kubala [37] first pointed out the correlation between ultimate bending strength and mineral content. Then the research about implanted biomaterials began to address the question how much strength was appropriate for bone tissue. In recent years, CPC has been used frequently in clinical application, where trabecular bones are directly exposed to CPC. For all kinds of CPC, their Young's modulus is not narrowly distributed around a constant value, but widespread over an extensive range of values [38–40]. Young's modulus of CPC is highlighted here, because it represents its inherent property [41]. The objective of this study is to investigate the response of bone tissue to CPC with different series of elastic modulus combinations.

The hydration behavior of CPC is a solution–precipitation process for phosphates, and the following neutralization reaction of acid and alkali acts as the driving force. Under different synthesis conditions, as-processed ACPs in our work showed different dissolution behaviors, which induced different hydration behaviors in the process of CPC setting, and then as-processed CPCs exhibited different duration of hardening and mechanical properties (Table 2). In FE modeling, two kinds of loading condition were applied on CPC/bone specimens (Fig. 2). The FE predictions demonstrated that elastic modulus of bone and CPC significantly affected their stress distribution. In mechanics, Von Mises Stress is generally used to describe strength. Compressive strength is used to describe material property with a uniaxial loading tension. Under the loading condition, Von Mises Stress in the sample can reflect the load-bearing capacity of specimen [42]. Under the strain mode, the Von Mises Stress is trending up with the increase of CPC's Young's modulus (Figs. 3 and 4). Figs. 4 and 5 exhibit that there is a larger stress at the interface of bone–CPC. This phenomenon is coincided with Tozzi's study [20], which reported that the largest loading stress occurred on the interface of bone and biomaterial.

Under the stress mode, the elastic modulus has a minor effect on the stress distribution of CPC (Figs. 6 and 7), and the stress value of bone tissue is larger than that of CPC. The most

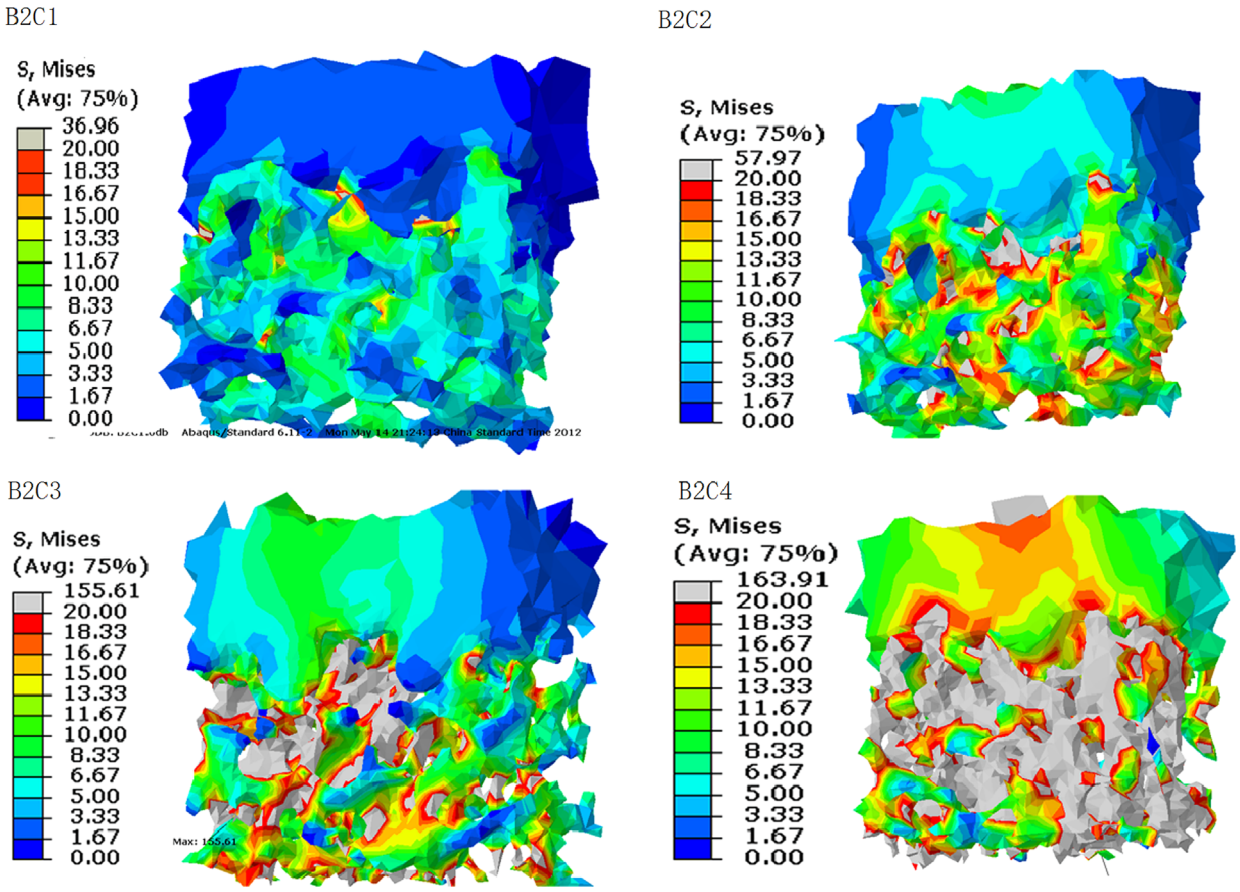

Fig. 4. The local predicted stress distributions on B2Cx series from the FE modeling under the loading condition A. Cx: C1-C4.

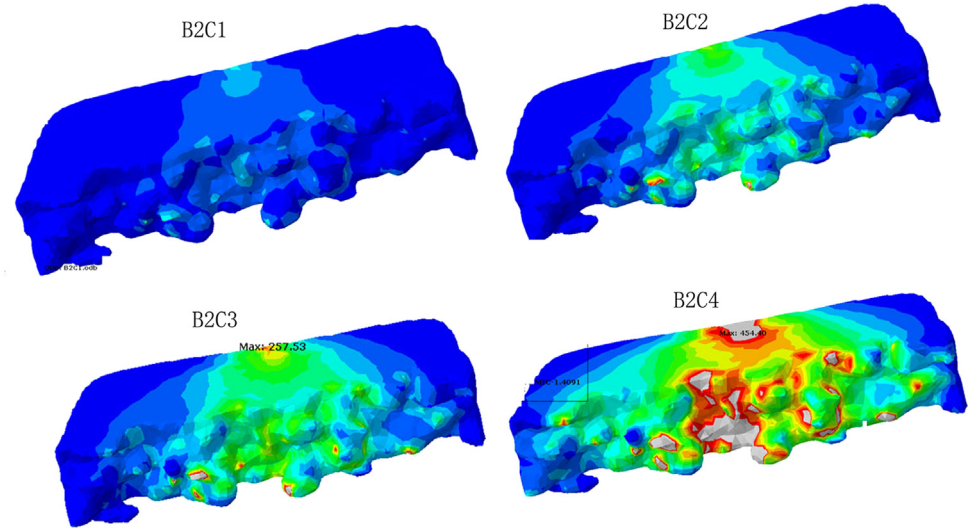

Fig. 5. The stress distributions in cement of B2Cx series from the FE modeling under the loading condition A.

stressed area of CPC is on the interface of bone–CPC, where the stress distribution is trending up with the increase of CPC's Young's modulus. When Young's modulus of CPC is relatively small, bone will be under more stress, which will increase the risk of second fracture of bone.

The quantitative analysis (Figs. 8–10) indicates that different transverse planes of bone–CPC specimen present different stress values. In CPC, the joint area of bone–CPC endures the largest stress. Under the surface pressure of 5 MPa, bone and CPC bear the same stress. In the joint area of bone–CPC, the stress on plane b1 is trending up with the increase of CPC's Young's modulus; but the stress on plane b2 is trending down with it. For all the bone–CPC combinations, B1C4 is the optimal one. The test results indicate that structure of material

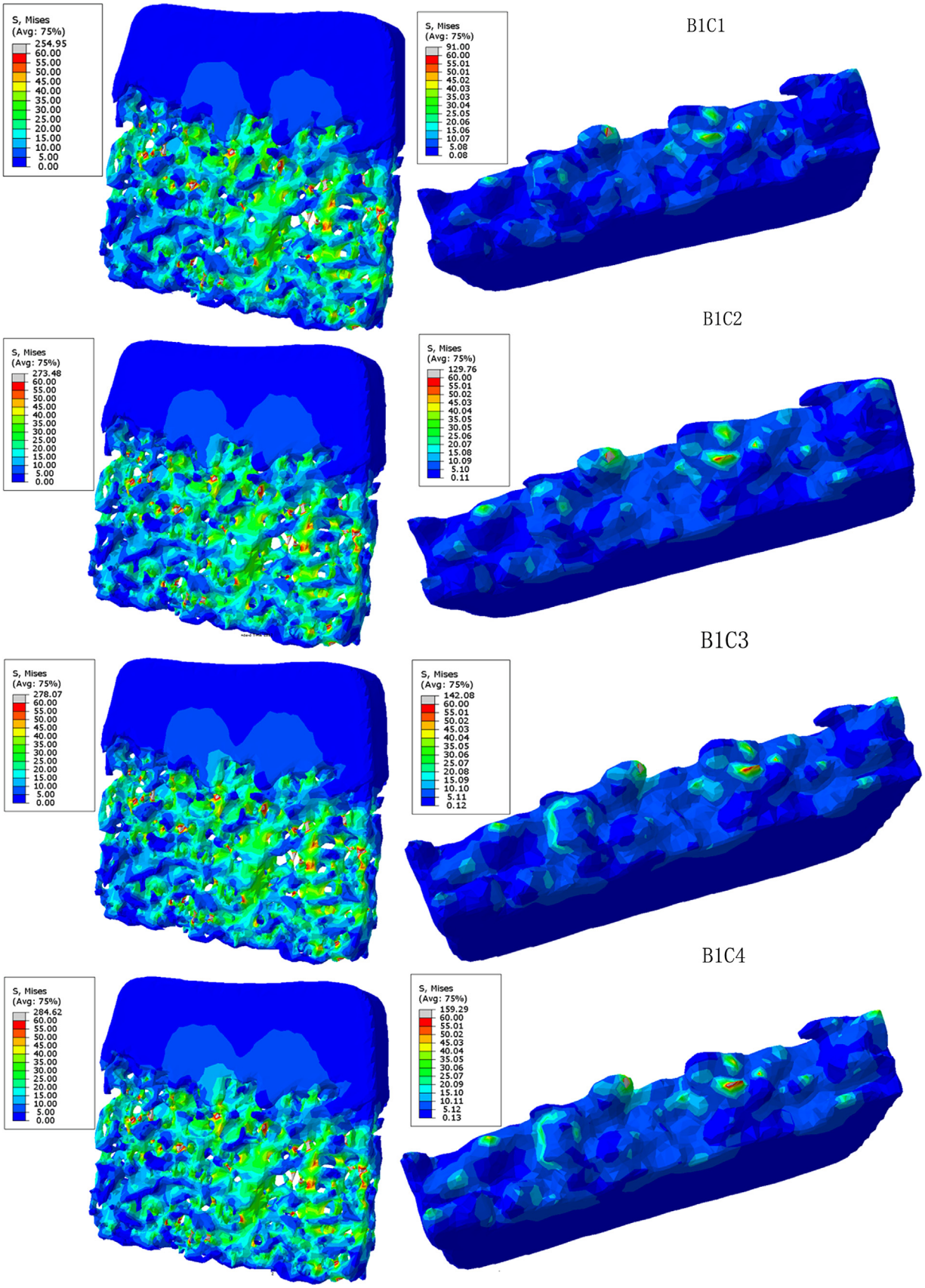

Fig. 6. The stress distributions on B1Cx series of specimen under the loading condition B.

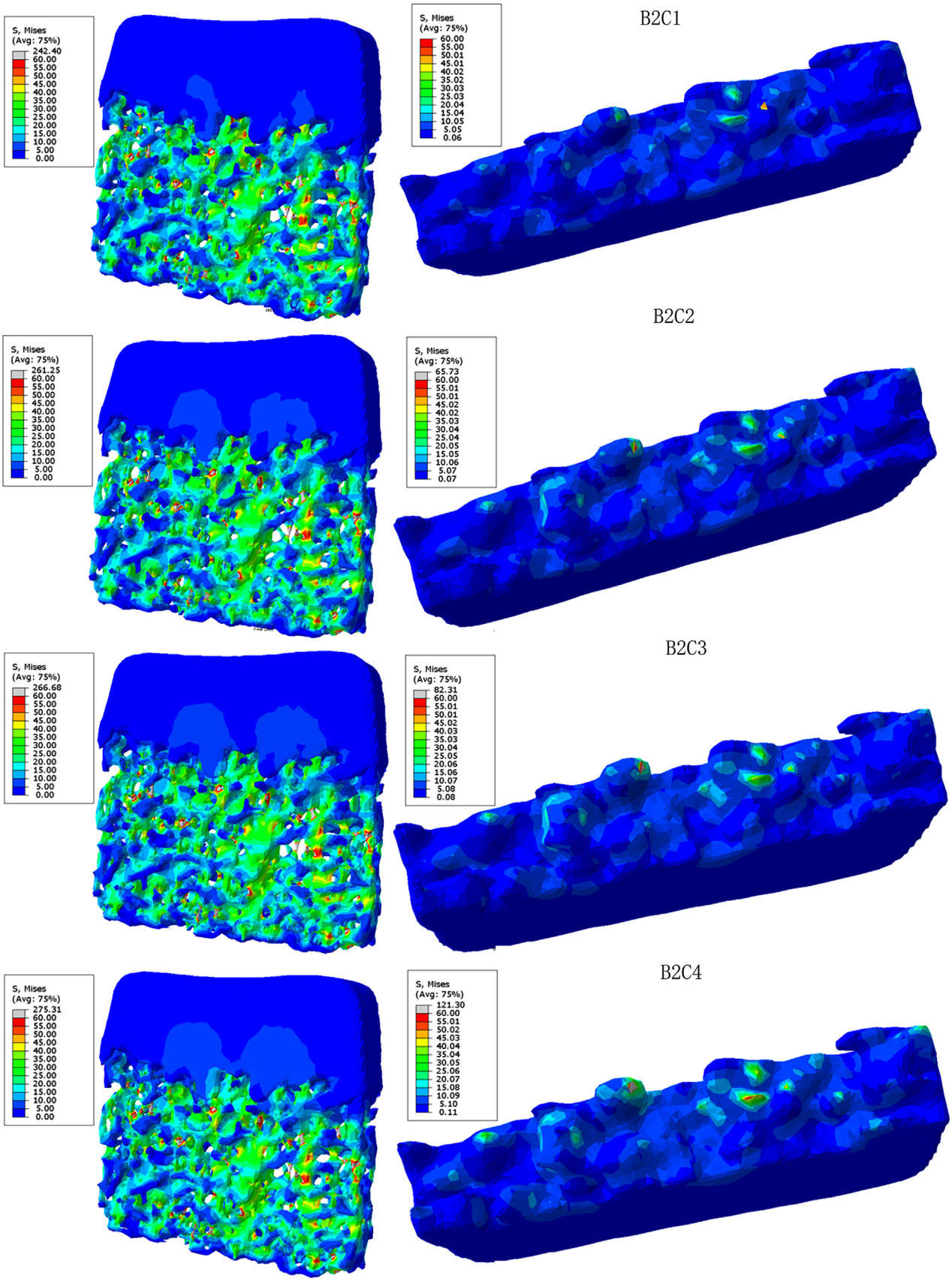

Fig. 7. The stress distributions on B2Cx series of specimen under the loading condition B.

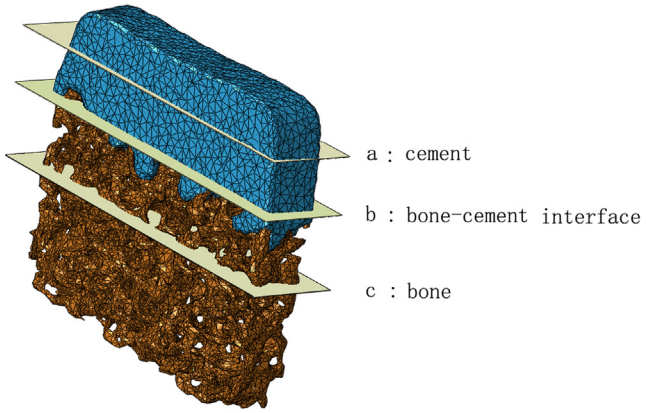

Fig. 8. The FE model of bone–cement sample: (a) cement; (b) bone–cement interface; (c) bone. In the FE analysis, three transverse planes were chosen to calculate the average stress and strain quantitatively. The average stress and strain = sum of the stresses and strains/number of total nodes for each transverse plane.

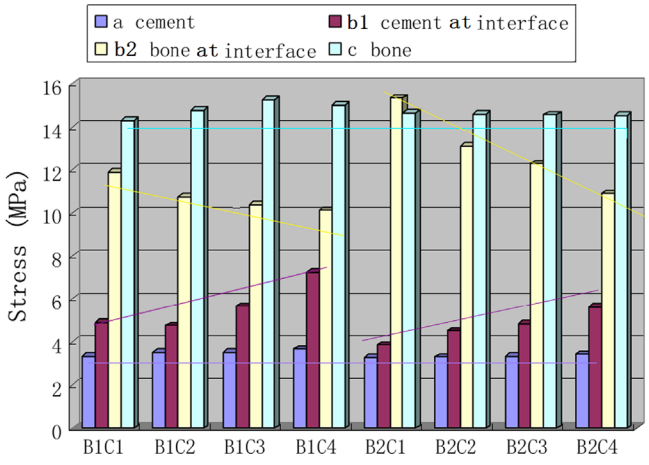

Fig. 9. The average stress in the transverse planes of the specimen predicted from FE modeling under the loading condition B.

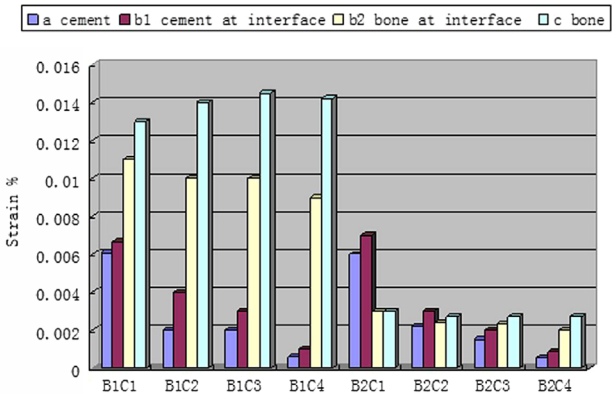

Fig. 10. The average strain in the different transverse planes of the specimen predicted from FE modeling under the loading condition B.

affects the stress distribution significantly. The average strain predicted by FE modeling in Fig. 10 indicates that higher elastic modulus induces less strain. All of these results indicated that FE modeling is the ideal method for predicting fracture behavior of bone–CPC specimen both qualitatively and quantitatively.

In 1892, Wolff first pointed out the relationship between bone structure and applied loads [43]. With different applied loads, bone was clearly anisotropic in both principal values of stiffness and direction changes, which was a remodeling process for bone except for the change in apparent density [44]. In sum, FE predictions indicate that Von Mises Stress of specimen correlates closely with elastic modulus of material. The mechanical properties of CPC can be adjusted by controlling the setting reaction of it. CPC will exhibit appropriate mechanical properties, by way of controlling the reactivity of CPC, so as to match the elastic modulus of bone tissue.

5. Conclusion

The results proved that FE modeling was an ideal method for predicting mechanical behavior of bone–CPC specimen both qualitatively and quantitatively. Structure of CPC and bone affected the stress distribution significantly. FE model exhibited that stress value of bone was greater than that of CPC under the same loading condition. For CPC, the interface of bone and CPC endured the largest stress, and there was a stress concentration on the interface. For all the bone–CPC combinations, B1C4 was the optimal one. FEA was proved to be an effective method to optimize the mechanical performance of implanted material in vivo. In addition, it was also possible to predict the initial stimuli of implanted material by FEA in our future researches, in order to analyze and propose a material design with a specific function.

Acknowledgments

This research was supported by National Natural Science Foundation of China, Grant number: 51172074; Natural Science Foundation of Guangdong Province of China, Grant number: 04205786; Hong Kong Scholars Program (XJ2011010); China Postdoctoral Science Foundation: 2012M511571; China Postdoctoral Science Foundation (CPSF): 201104358; Guangdong Natural Science Foundation: S2012040007845; Fundamental Research Funds for the Central Universities (2013ZZ0010); National Natural Science Foundation of China (51302089).

References

[1] B. Han, P. Ma, L. Zhang, Y. Yin, beta-TCP/MCPM-based premixed calcium phosphate cements, Acta Biomater. 5 (2009) 3165–3177.
[2] J.A. Youssef, V.M. Salas, R.G. Loschiavo, Management of painful osteoporotic vertebral compression fractures: vertebroplasty and kyphoplasty, Oper. Tech. Orthop. 13 (2003) 222–226.
[3] J.A. Carrino, R. Chan, A.R. Vaccaro, Vertebral augmentation: vertebroplasty and kyphoplasty, Semin. Roentgenol. 39 (2004) 68–84.
[4] A.G. Hadjipavlou, M.N. Tzermiadianos, P.G. Katonis, M. Szpalski, Percutaneous vertebroplasty and balloon kyphoplasty for the treatment of vertebral compression fractures and osteolytic tumors, J. Bone Joint Surg. Br. 87 (2005) 1595–1604.

[5] C.S. Liu, H.F. Shao, F.Y. Chen, H.Y. Zheng, Effects of the granularity of raw materials on the hydration and hardening process of calcium phosphate cement, Biomaterials 24 (2003) 4103–4113.
[6] R.C. Thomson, M.J. Yaszemski, J.M. Powers, A.G. Mikos, Hydroxyapatite fiber reinforced poly (a-hydroxyester) foams for bone regeneration, Biomaterials 19 (1998) 1935–1943.
[7] P. Ducheyne, Q. Qiu, Bioactive ceramics: the effect of surface reactivity on bone formation and bone cell function, Biomaterials 20 (1999) 2287–2303.
[8] R.M. Pilliar, M.J. Filiaggi, J.D. Wells, M.D. Grynpas, R.A. Kandel, Porous calcium polyphosphate scaffolds for bone substitute applications-in vitro characterization, Biomaterials 22 (2001) 963–972.
[9] E. Fernández, M.P. Ginebra, O. Bermudez, M.G. Boltong, F.C. M. Driessens, J.A. Planell, Dimensional and thermal behaviour of calcium phosphate cements during setting compared to PMMA bone cements, J. Mater. Sci. Lett. 14 (1995) 4–5.
[10] K. Takahashi, Y. Fujishiro, S. Yin, T. Sato, Preparation and compressive strength of alpha-tricalcium phosphate based cement dispersed with ceramic particles, Ceram. Int. 30 (2004) 199–203.
[11] X.P. Wang, J.D. Ye, Y.J. Wang, L. Chen, Reinforcement of calcium phosphate cement by bio-mineralized carbon nanotube, J. Am. Ceram. Soc. 90 (2007) 962–964.
[12] H.H.K. Xu, F.C. Eichmiller, A.A. Giuseppetti, Reinforcement of a self setting calcium phosphate cement with different fibers, J. Biomed. Mater. Res. 52 (2000) 107–114.
[13] E.F. Burguera, H.H.K. Xu, S. Takagi, L.C. Chow, High early strength calcium phosphate bone cement: effects of dicalcium phosphate dihydrate and absorbable fibers, J. Biomed. Mater. Res. A 75 (2005) 966–975.
[14] Y. Zhang, H.H.K. Xu, Effects of synergistic reinforcement and absorbable fiber strength on hydroxyapatite bone cement, J. Biomed. Mater. Res. A 75 (2005) 832–840.
[15] H. Yamamoto, S. Niwa, M. Hori, et al., Mechanical strength of calcium phosphate cement in vivo and in vitro, Biomaterials 19 (1998) 1587–1591.
[16] A.E. Goodship, J.L. Cunningham, Pathophysiology of functional adaptation of bone in remodeling and repair in vivo, in: SC Cowin (Ed.), Bone Mechanics Handbook, 2nd ed., CRC Press, Boca Raton, FL, 2001, pp. 261–263.
[17] C.H. Turner, Three rules for bone adaptation to mechanical stimuli, Bone 23 (1998) 399–407.
[18] M.C.H. van der Meulen, R. Huiskes, Why mechanobiology? A survey article, J. Biomech. 35 (2002) 401–414.
[19] G. Tozzi, Q.H. Zhang, J. Tong, 3D real-time micromechanical compressive behaviour of bone–cement interface: experimental and finite element studies, J. Biomech. 45 (2012) 356–363.
[20] A. Pegoretti, L. Fambri, G. Zappini, M. Bianchetti, Finite element analysis of a glass fibre reinforced composite endodontic post, Biomaterials 13 (23) (2002) 2667–2682.
[21] P. Miranda, A. Pajares, F. Guiberteau, Finite element modeling as a tool predicting the fracture behavior of robocast scaffolds, Acta Biomaterialia 4 (2008) 1715–1724.
[22] D. Lacroix, A. Chateau, M.P. Ginebra, J.A. Planell, Micro-finite element models of bone tissue-engineering scaffold, Biomaterials 27 (2006) 5326–5334.
[23] T. Yu, J.D. Ye, Y.J. Wang, Control of crystallinity of hydrated products in a calcium phosphate cement, J. Am. Ceram. Soc. 92 (4) (2009) 949–951.
[24] K.W. Luczynski, A. Dejaco, O. Lahayne, J. Jaroszewicz, W. Swieszkowski, C. Hellmich, MicroCT/micromechanics-based finite element models and quasi-static unloading tests deliver consistent values for Young's modulus of rapid-prototyped polymer-ceramic tissue engineering scaffold, Comput. Model. Eng. Sci. 87 (6) (2012) 505–528.
[25] K. Zainali, G. Danscher, T. Jakobsen, J. Baas, P. Moller, J.E. Bechtold, K. Soballe, Assessment of modified gold surfaced titanium implants on skeletal fixation, J. Biomed. Mater. Res. Pt A 101A (1) (2013) 195–202.
[26] S. Scheiner, R. Sinibaldi, B. Pichler, V. Komlev, C. Renghini, C. Vitale-Brovarone, F. Rustichelli, C. Hellmich, Micromechanics of bone tissue-engineering scaffolds, based on resolution error-cleared computer tomography, Biomaterials 30 (2009) 2411–2419.
[27] A. Dejaco, V.S. Komlev, J. Jaroszewicz, W. Swieszkowski, C. Hellmich, Micro CT-based multiscale elasticity of double-porous (pre-cracked) hydroxyapatite granules for regenerative medicine, J. Biomech. 45 (2012) 1068–1075.
[28] T.M. Keaveny, E.F. Wachtel, C.M. Ford, W.C. Hayes, Differences between the tensile and compressive strengths of bovine tibial trabecular bone depend on modulus, J. Biomech. 27 (1994) 1137–1146.
[29] J.L. Stone, G.S. Beaupre, W.C. Hayes, Multiaxial strength characteristics of trabecular bone, J. Biomech. 9 (1983) 743–752.
[30] B. van Rietbergen, H. Weinans, R. Huiskes, A. Odgaard, A new method to determine trabecular bone elastic properties and loading using micromechanical finite-elements methods, J. Biomech. 28 (1995) 69–81.
[31] W.E. Brown, L.C. Chow, A new calcium phosphate, water-setting cement, in: PW Brown (Ed.), Cements Research Progress, American Ceramic Society, Westerville, OH, 1986, pp. 352–379.
[32] L.C. Chow, Development of self-setting CPCs, J. Ceram. Soc. Jpn. 99 (1991) 954–964.
[33] P.W. Brown, Hydration behavior of calcium phosphates is analogous to hydration behavior of calcium silicates, Cem. Concr. Res. 29 (1999) 1167–1171.
[34] T. Yu, J.D. Ye, Y.J. Wang, Preparation and characterization of a novel strontium-containing calcium phosphate cement with the two-step hydration process, Acta Biomater. 5 (2009) 2717–2727.
[35] H. Gong, M. Zhang, L. Qin, Y.J. Hou, Regional variations in the apparent and tissue-level mechanical parameters of vertebral trabecular bone with aging using micro-finite element analysis, Ann. Biomed. Eng. 35 (9) (2007) 1622–1631.
[36] M. Doblare, J.M. Garcia, M.J. Gomez, Modelling bone tissue fracture and healing: a review, Eng. Fract. Mech. 71 (2004) 1809–1840.
[37] G.P. Vose, A.L. Kubala, Bone strength – its relationship to X-ray-determined ash content, Hum. Biol. 31 (1959) 261–270.
[38] K. Ishikawa, K. Asaoka, Estimation of ideal mechanical strength and critical porosity of calcium phosphate cement, J. Biomed. Mater. Res. 29 (1995) 1537–1543.
[39] E. Charrière, S. Terrazzoni, C. Pittet, et al., Mechanical characterization of brushite and hydroxyapatite cements, Biomaterials 22 (2001) 2937–2945.
[40] H. Morgan, R.H. Dauskardt, Notch strength insensitivity of self-setting hydroxyapatite bone cements, J. Mater. Sci. Mater. Med. 14 (2003) 647–653.
[41] B.D. Ratner, A.S. Hoffman, F.J. Schoen, J.E. Lemons, Biomaterials Science: An Introduction to Materials in Medicine, 2nd edition, Elsevier, San Diego, C.A., 2004, p. 28.
[42] H. Gong, Y.B. Fan, M. Zhang, L. Qin, Age-and direction-related adaptations of lumbar vertebral trabecular bone with respect to apparent stiffness and tissue level stress distribution, Acta Mech. Sin. 25 (1) (2009) 121–129.
[43] J. Wolff, Das Gesetz der Transformation der Knochen, Berlin, Hirschwald, 1892.
[44] S.C. Cowin, Wolff's law of trabecular architecture at remodeling equilibrium, J. Biomech. Eng. 108 (1986) 83–88.
[45] ABAQUS, ABAQUS User's Manual, Version 6.11. Dassault Systemes Simulia Corp, Providence, RI, USA, 2011.